2005

Crystal Growth, Structural Transitions, and Magnetic Properties of the Fluorite-Related Osmates: Sm3OsO7, Eu3OsO7, and Gd3OsO7

William R. Gemmill
University of South Carolina

Mark D. Smith
University of South Carolina

Yurij Mozharivskyj
Iowa State University

Gordon J. Miller
Iowa State University, gmiller@iastate.edu

Hans-Conrad zur Loye
University of South Carolina

Crystal Growth, Structural Transitions, and Magnetic Properties of the Fluorite-Related Osmates: Sm3OsO7, Eu3OsO7, and Gd3OsO7

Abstract
The Ln_3OsO_7 (Ln = Sm, Eu, Gd) compounds were grown as single crystals from molten hydroxide fluxes. At temperatures above 235, 330, and 430 K, respectively, the Ln_3OsO_7 (Ln = Sm, Eu, Gd) compounds exist in the orthorhombic space group *Cmcm*. When they are cooled below these temperatures, the compounds undergo a structural phase transition from space group *Cmcm* to $P2_1nb$. The structure transition results in a loss of lattice centering, a doubling of the *b* axis, a distortion of the vertex-shared Os−O chains, and a reduction in the coordination of one of the rare earth cations from 8-fold to 7-fold. Sm_3OsO_7 and Eu_3OsO_7 exhibit complex magnetic behavior below about 50 K, and Gd_3OsO_7 shows a ferromagnetic-like order at 34 K in applied fields of less than 10 kG.

Disciplines
Materials Chemistry | Other Chemistry | Physical Chemistry

Inorg. Chem. **2005**, *44*, 7047–7055

Crystal Growth, Structural Transitions, and Magnetic Properties of the Fluorite-Related Osmates: Sm_3OsO_7, Eu_3OsO_7, and Gd_3OsO_7

William R. Gemmill,[†] Mark D. Smith,[†] Yurij A. Mozharivsky,[@] Gordon J. Miller,[#] and Hans-Conrad zur Loye*,[†]

Department of Chemistry and Biochemistry, University of South Carolina, Columbia, South Carolina 29208, Ames Laboratory, Iowa State University, Ames, Iowa 50011-3020, and Department of Chemistry, Iowa State University, Ames, Iowa 50011-3110

Received April 20, 2005

The Ln_3OsO_7 (Ln = Sm, Eu, Gd) compounds were grown as single crystals from molten hydroxide fluxes. At temperatures above 235, 330, and 430 K, respectively, the Ln_3OsO_7 (Ln = Sm, Eu, Gd) compounds exist in the orthorhombic space group *Cmcm*. When they are cooled below these temperatures, the compounds undergo a structural phase transition from space group *Cmcm* to $P2_1nb$. The structure transition results in a loss of lattice centering, a doubling of the *b* axis, a distortion of the vertex-shared Os–O chains, and a reduction in the coordination of one of the rare earth cations from 8-fold to 7-fold. Sm_3OsO_7 and Eu_3OsO_7 exhibit complex magnetic behavior below about 50 K, and Gd_3OsO_7 shows a ferromagnetic-like order at 34 K in applied fields of less than 10 kG.

Introduction

The crystal growth of complex metal oxides containing both a lanthanide and a platinum group metal remains a challenge, although recent advances in the use of molten hydroxides as growth media have resulted in the synthesis of several new oxide materials.[1−6] The acid−base chemistry of hydroxides, described by the Lux−Flood acid−base definition[7,8] allows for a wide range of species to be present in solution, making them a versatile solvent for crystal growth. In fact, it has been known for some time that molten hydroxides are an excellent solvent of crystallization for lanthanide containing oxides,[9,10] where the solubility of the lanthanides is dictated by the acid−base properties of the melt. Specifically, the water content of the melt must be controlled to enable the dissolution of the lanthanide oxides (Ln_2O_3),[7,8,11] which are only soluble in acidic "wet" melts.[10] We have recently shown that such wet melts are one route for the growth of oxide single crystals containing both lanthanide and platinum group metals (Ru, Rh, Pd, Os, Ir, Pt).[1−4,6]

As part of our investigation of the Ln−M−O (Ln = lanthanide, M = platinum group metal) phase space, we have been systematically studying the reaction between lanthanides and platinum group metals using molten hydroxide solvents and have shown that, as a function of the lanthanide size, single crystals of complex oxides with different structure types form. For example, in the Ln−Ru−O phase space, single crystals of the double perovskite, Ln_2NaRuO_6, are obtained for the larger lanthanides (Ln = La, Pr, Nd),[4] while for the smaller lanthanides (Ln = Sm, Eu), single crystals of the fluorite-related structure, Ln_3RuO_7, are formed.[5] Analogously, the Ln−Os−O phase space also allows for the isolation of single crystals of the double perovskites, Ln_2NaOsO_6, for the larger lanthanides (Ln = La, Pr, Nd)[3], and the formation of single crystals of the fluorite-related structure, Ln_3OsO_7, for the smaller lanthanides (Ln = Sm, Eu, Gd) (this article). The polycrystalline powder preparation and magnetic properties of Ln_3OsO_7 (Ln = La, Pr, Nd, Sm),[12,13] have been previously reported.

* To whom correspondence should be addressed. E-mail: zurloye@mail.chem.sc.edu.
[†] Department of Chemistry and Biochemistry, University of South Carolina.
[@] Ames Laboratory, Iowa State University.
[#] Department of Chemistry, Iowa State University.

(1) Davis, M. J.; Mugavero, S. J.; Glab, K. I.; Smith, M. D.; zur Loye, H.-C. *Solid State Sci.* **2004**, *5*, 413.
(2) Davis, M. J.; Smith, M. D.; zur Loye, H.-C. *Inorg. Chem.* **2003**, *42*, 6980.
(3) Gemmill, W. R.; Smith, M. D.; Prozorov, R.; zur Loye, H.-C. *Inorg. Chem.* **2005**, *44*, 2639.
(4) Gemmill, W. R.; Smith, M. D.; zur Loye, H.-C. *J. Solid State Chem.* **2004**, *177*, 3560.
(5) Gemmill, W. R.; Smith, M. D.; zur Loye, H.-C. *Inorg. Chem.* **2004**, *43*, 4254.
(6) Mugavero, S. J.; Smith, M. D.; zur Loye, H.-C. *J. Solid State Chem.* **2004**, *178*, 200.
(7) Flood, H.; Forland, T. *Acta Chem. Scand.* **1947**, *1*, 592.
(8) Lux, H. *Z. Elektrochem.* **1939**, *45*, 303.
(9) Luce, J. L.; Stacy, A. M. *Chem. Mater.* **1997**, *9*, 1508.
(10) Keller, S. W.; Carlson, V. A.; Sanford, D.; Stenzer, F.; Stacy, A. M.; Kwei, G. H.; Alario-Franco, M. *J. Am. Chem. Soc.* **1994**, *116*, 8070.
(11) Goret, J. *Bull. Soc. Chim.* **1964**, 1074.

10.1021/ic0506106 CCC: $30.25
Published on Web 09/02/2005

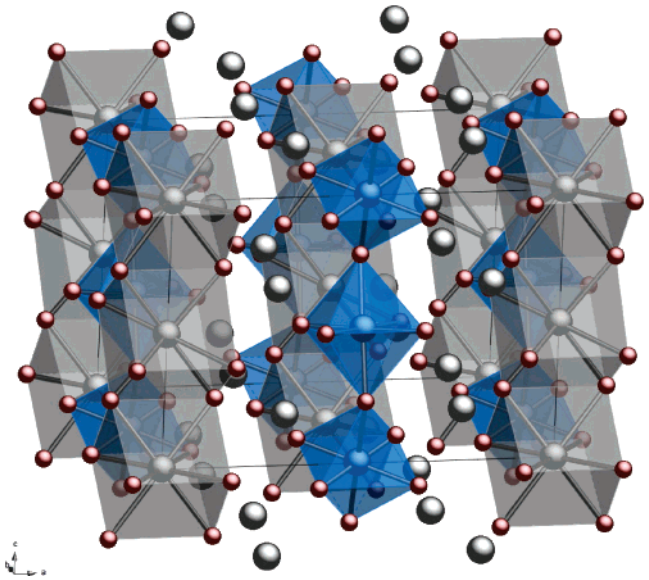

Figure 1. Drawing of the *Cmcm* structure of Ln_3OsO_7 (Ln = Sm, Eu, Gd) emphasizing the chains of trans vertex-sharing OsO_6 octahedra (blue) that are edge shared to chains of $Ln(1)O_8$ pseudo-cubes (gray) along the *c* axis. The gray spheres are the $Ln(2)^{3+}$ cations.

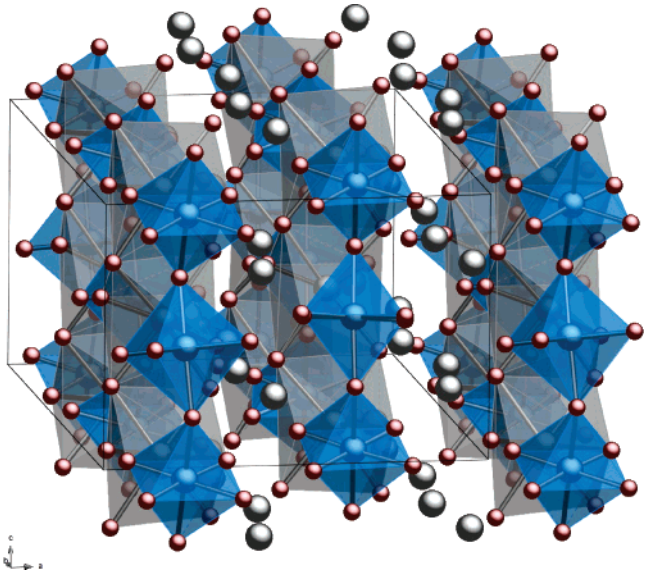

Figure 2. Drawing of the low temperature $P2_1nb$ structure of Ln_3OsO_7 (Ln = Sm, Eu, Gd) emphasizing the chains of trans vertex-sharing OsO_6 octahedra that are edge shared to chains of $Ln(1, 2)O_7$ mono-capped trigonal prisms along the *c* axis. The spheres are the $Ln(3-6)^{3+}$ cations.

The family of compounds of the general formula Ln_3MO_7, where Ln is a lanthanide and M is a pentavalent metal cation, were first reported by Allpress and Rossell in 1979 and were described as having an orthorhombic fluorite-related structure.[14] Since then, many compositions have been prepared and investigated, including Ln_3MO_7 (Ln = La, Pr, Nd; M = Nb, Ta, Sb),[14−17] Ln_3RuO_7 (Ln = La, Pr, Nd, Sm, Eu, Gd),[5,18−22] Ln_3ReO_7 (Ln = La, Pr, Nd, Sm, Gd, Tb, Dy),[23−25] Ln_3OsO_7 (Ln = La, Pr, Nd, Sm),[12,13] and Ln_3IrO_7 (Ln = Pr, Nd, Sm, Eu)[26,27] The structure of these compounds is well described in the orthorhombic space group *Cmcm* and features chains of trans vertex-sharing MO_6 octahedra that are oriented along the *c* axis and that are tilted in the *bc* plane. In this structure, the lanthanide cations are located in two different coordination environments, 8-fold pseudo-cubic and 7-fold pentagonal bipyramidal, and the M(V) cations are located in octahedral coordination. (Figure 1). Detailed magnetic and thermal investigations have been reported for the ruthenium- and iridium-containing members of this family, which have provided evidence for the existence of low-temperature structural phase transitions and, moreover, revealed that the transition temperature is a function of the specific lanthanide ion in the Ln_3MO_7 (M = Ir, Ru) oxides.[27−31] To elucidate the structure of the low-temperature phase, we recently reported on the Ln_3RuO_7 (Ln = Sm, Eu)[5] compounds where we described the observed structural phase transition from space group *Cmcm* to $P2_1nb$. The structure transition results in a distortion of the vertex-shared Ru−O chains and a reduction in the coordination of one of the rare earth cations from 8-fold to 7-fold, in addition to a loss of lattice centering and doubling of the *b* axis. (Figure 2). Herein, we report the observation of the analogous structural phase transitions in Sm_3OsO_7, Eu_3OsO_7, and Gd_3OsO_7 where, below the temperatures of approximately 235, 330, and 430 K, respectively, they exist in the low-temperature $P2_1nb$ structure and upon heating undergo a structural phase transition to the high-temperature *Cmcm* structure as determined from a combination of single-crystal X-ray diffraction and TGA-DTA analysis. In this paper, we report on the high- and low-temperature crystal structures of Sm_3OsO_7, Eu_3OsO_7, and Gd_3OsO_7, as well as on the magnetic properties of these oxides.

Experimental Section

Crystal Growth. For the Ln_3OsO_7 (Ln = Sm, Eu, Gd) compounds, 1.00 mmol of Os metal (J & J Materials, Inc., 99.98%),

(12) Plaisier, J. R.; Drost, R. J.; IJdo, D. J. W. *J. Solid State Chem.* **2002**, *169*, 189.
(13) Lam, R.; Wiss, F.; Greedan, J. E. *J. Solid State Chem.* **2002**, *167*, 182.
(14) Allpress, J. G.; Rossell, H. J. *J. Solid State Chem.* **1979**, *27*, 105.
(15) Kahn-Harari, A.; Mazerolles, L.; Michel, D.; Robert, F. *J. Solid State Chem.* **1995**, *116*, 103.
(16) Rossell, H. J. *J. Solid State Chem.* **1979**, *27*, 115.
(17) Rossell, H. J. *J. Solid State Chem.* **1979**, *27*, 287.
(18) Bontchev, R. P.; Jacobson, A. J.; Gospodinov, M. M.; Skumryev, V.; Popov, V. N.; Lorenz, B.; Meng, R. L.; Litvinchuk, A. P.; Iliev, M. N. *Phys. Rev. B: Condens. Matter Mater. Phys.* **2000**, *62*, 12235.
(19) Khalifah, P.; Erwin, R. W.; Lynn, J. W.; Huang, Q.; Batlogg, B.; Cava, R. J. *Phys. Rev. B* **1999**, *60*, 9573.
(20) Khalifah, P.; Huang, Q.; Lynn, J. W.; Erwin, R. W.; Cava, R. *J. Mater. Res. Bull.* **2000**, *35*, 1.
(21) Wiss, F.; Raju, N. P.; Wills, A. S.; Greedan, J. E. *Int. J. Inorg. Mater.* **2000**, *2*, 53.
(22) van Berkel, F. P. F.; IJdo, D. J. W. *Mater. Res. Bull.* **1986**, *21*, 1103.
(23) Lam, R.; Langet, T.; Greedan, J. E. *J. Solid State Chem.* **2003**, *171*, 317.
(24) Wltschek, G.; Paulus, H.; Svoboda, I.; Ehrenberg, H.; Fuess, H. *J. Solid State Chem.* **1996**, *125*, 1.
(25) Hinatsu, Y.; Wakeshima, M.; Kawabuchi, N.; Taira, N. *J. Alloys Compd.* **2004**, *374*, 79.
(26) Vente, J. F.; Ijdo, D. J. W. *Mater. Res. Bull.* **1991**, *26*, 1255.
(27) Nishimine, H.; Wakeshima, M.; Hinatsu, Y. *J. Solid State Chem.* **2004**, *177*, 739.
(28) Harada, D.; Hinatsu, Y. *J. Solid State Chem.* **2001**, *158*, 245.
(29) Harada, D.; Hinatsu, Y.; Ishii, Y. *J. Phys.: Condens. Matter* **2001**, *13*, 10825.
(30) Harada, D.; Hinatsu, Y. *J. Solid State Chem.* **2002**, *164*, 163.
(31) Greedan, J. E.; Raju, N. P.; Wegner, A.; Gougeon, P.; Padiou, J. *J. Solid State Chem.* **1997**, *129*, 320.

Table 1. Crystallographic Data and Structure Refinement for the *Cmcm* Structure of Ln_3OsO_7 (Ln = Sm, Eu, Gd)

	Sm_3OsO_7	Eu_3OsO_7	Gd_3OsO_7
fw (g/mol)	753.25	758.08	773.95
space group	*Cmcm*	*Cmcm*	*Cmcm*
temp (K)	294	380	480
unit cell dimensions			
a (Å)	10.7627(4)	10.7338(16)	10.673(3)
b (Å)	7.3772(3)	7.3872(11)	7.404(2)
c (Å)	7.4558(3)	7.4544(11)	7.423(2)
V (Å^3)	591.98(4)	591.08(15)	586.6(3)
Z	4	4	4
density$_{calcd}$ (mg m^{-3})	8.452	8.519	8.764
abs coeff (mm$^{-1)}$	50.696	52.803	55.047
reflns collected	1272	1599	1296
independent reflns	597 (R_{int} = 0.0446)	401 (R_{int} = 0.0292)	386 (R_{int} = 0.0348)
GOF on F^2	1.175	1.145	1.181
final R indices [$I > 2\sigma(I)$]	R1 = 0.0269, wR2 = 0.0590	R1 = 0.0204, wR2 = 0.0470	R1 = 0.0219, wR2 = 0.0558
R indices (all data)	R1 = 0.0280, wR2 = 0.0596	R1 = 0.0214, wR2 = 0.0474	R1 = 0.0228, wR2 = 0.0562
extinction coeff	0.00229(14)	0.00213(9)	0.00227(13)
residual electron density (e$^-$ Å^{-3})	1.789 and −3.148	2.227 and −1.246	1.884 and −1.556

1.5 mmol of Ln_2O_3 (Alfa Aesar, REaction, 99.9%), a 10-fold mass excess of NaOH (Fisher, ACS reagent) and 0.5 g of H_2O were placed into a silver tube that had been flame sealed on one end. The silver tube was then crimped shut on the other end, placed into a box furnace, and heated to the reaction temperature of 600 °C at 10 °C/min. The reaction was held at temperature for 12 h and then cooled to room temperature by turning off the furnace. The flux was dissolved with water aided by the use of sonication followed by manual isolation of the crystals.

Single-Crystal X-ray Diffraction. All single-crystal X-ray diffraction experiments were carried out using Bruker SMART APEX CCD-based diffractometer (graphite-monochromated Mo Kα radiation, λ = 0.71073 Å). Integrated intensities were extracted from the raw area-detector data and corrected for Lorentz and polarization effects with SAINT+.[32] Empirical absorption corrections based on the multiple measurement of equivalent reflections were applied to each data set with SADABS.[32] A full-matrix least-squares refinement of the known structural models for the high- and low-temperature forms was performed against F^2 with SHELXTL.[37]

Room- and High-Temperature X-ray Diffraction. For the high-temperature X-ray diffraction data (T > 294 K), the diffractometer was fitted with a Nonius crystal heater.[33] The data crystals were mounted on glass capillaries with epoxy. The crystal of Eu_3OsO_7 was heated to 380 K and that of Gd_3OsO_7 to 480 K by a stream of hot argon, above their transition temperatures. During the data collections, the temperature was stable to within ±1 K of the value set for the experiment. Diffraction data covering a hemisphere of reciprocal space were harvested with 0.3° scans in ω and with an exposure time of 10 s per frame to $2\theta_{max}$ = 57°. A suitable crystal of Sm_3OsO_7 was epoxied onto a thin glass fiber for the room-temperature measurement. The data collection covered ca. 85% of the full sphere of reciprocal space to $2\theta_{max}$ = 65°. For all compounds, refinement of the data in the space group *Cmcm*, known for the high-temperature form of the compounds, converged rapidly. All atoms were refined with anisotropic displacement parameters. Refinement of the site occupation factors for the metal atoms showed no deviation from unity occupancy in any case. Final refinement statistics for the room- and high-temperature data sets are compiled in Table 1.

Low-Temperature Single-Crystal X-ray Diffraction. When the crystals of Sm_3OsO_7 were cooled below ca. 235 K, additional reflections appeared in the diffraction pattern. Though weak, all additional diffraction peaks could be indexed to a primitive orthorhombic cell with $a \approx 10.7$ Å, $b \approx 14.6$ Å, and c ≈ 7.4 Å, corresponding to a doubling of the *b* axis of the high-temperature *Cmcm* cell and a loss of lattice centering. This observation corresponds exactly to the structural transition previously observed in crystals of the ruthenium analogues Ln_3RuO_7 (Ln = Sm, Eu).[5] The transition temperatures of Eu_3OsO_7 and Gd_3OsO_7 were not determined by diffraction techniques. Data sets with high redundancy were collected at 100 K for Sm_3OsO_7 and at 150 K for Eu_3OsO_7 and Gd_3OsO_7 to $2\theta_{max} \geq 65°$. Systematic absences in the low-temperature intensity data sets indicated the space groups *Pmnb* and $P2_1nb$ (the nonstandard settings of *Pnma* and $Pna2_1$). The acentric space group $P2_1nb$ was initially assumed by analogy to Ln_3RuO_7 (Ln = Sm, Eu). Refinement in the $P2_1nb$ space group of the structural models from the low-temperature forms of Ln_3RuO_7 (Ln = Sm, Eu) yielded satisfactory results. Trial refinements in the *Pmnb* space group resulted in physically unreasonable displacement parameters and difference map features, as well as high *R* factors, thereby confirming $P2_1nb$. All data sets were refined as perfect inversion twins, as with the ruthenates. The metal atoms were refined with anisotropic displacement parameters except for atoms Sm3, Sm6, and Eu6 from the appropriate data sets. All oxygen atoms were refined isotropically. The final refinement statistics for the low-temperature data sets for Eu_3OsO_7, Gd_3OsO_7, and for Sm_3OsO_7 are compiled in Table 4.

Scanning Electron Microscopy. Environmental scanning electron micrographs (ESEM) of several single crystals were obtained using a FEI Quanta 200 ESEM instrument utilized in the low-vacuum mode. Energy dispersive spectroscopy (EDS) verified the presence of samarium, osmium, and oxygen in Sm_3RuO_7, europium, osmium, and oxygen in Eu_3OsO_7, and gadolinium, osmium, and oxygen in Gd_3OsO_7. Furthermore, within the detection limit of the instrument, no extraneous elements were detected.

Differential Thermal Analysis/Thermogravimetric Analysis (DTA-TGA). Thermogravimetric analyses were carried out on a TA Instruments SDT 2960 simultaneous DTA-TGA by heating the

(32) *SMART*, version 5.625, *S. V.*, and *SADABS*, version 2.05; Bruker Analytical X-ray Systems, Inc.: Madison, WI, 2001.
(33) Tuinstra, F.; Storm, G. M. F. *J. Appl. Crystallogr.* **1978**, *11*, 257.
(34) Reading, J.; Gordeev, S.; Weller, M. T. *J. Mater. Chem.* **2002**, *12*, 646.
(35) Treiber, V. U.; Kemmler-Sack, S. *Z. Anorg. Allg. Chem.* **1981**, *478*, 223.
(36) Wiebe, C. R.; Gourrier, A.; Langet, T.; Britten, J. F.; Greedan, J. E. *J. Solid State Chem.* **2000**, *151*, 31.
(37) Sheldrick, G. M. *SHELXTL*; Bruker Analytical X-ray Systems, Inc.: Madison WI, 1997.

Table 2. Atomic Coordinates and Equivalent Isotropic Parameters for the *Cmcm* Structures of Ln_3OsO_7 (Ln = Sm, Eu, Gd)

	x	*y*	*z*	U_{eq} (Å^2)
		Sm_3OsO_7		
Sm(1)	0	0	0	0.015(1)
Sm(2)	0.2261(1)	0.3001(1)	1/4	0.010(1)
Os	0	1/2	0	0.008(1)
O1	0.1274(5)	0.3147(7)	−0.0371(5)	0.019(1)
O2	0.1318(5)	0.0252(8)	0.2500	0.011(1)
O3	0	0.4199(12)	0.2500	0.011(1)
		Eu_3OsO_7		
Eu(1)	0	0	0	0.0138(2)
Eu(2)	0.2264(9)	0.2990(1)	1/4	0.0072(2)
Os	0	1/2	0	0.0043(2)
O1	0.1267(6)	0.3141(9)	−0.0384(7)	0.020(1)
O2	0.1329(7)	0.0263(11)	1/4	0.009(2)
O3	0	0.4173(15)	1/4	0.010(2)
		Gd_3OsO_7		
Gd(1)	0	0	0	0.0171(3)
Gd(2)	0.22656(5)	0.29684(8)	1/4	0.0079(5)
Os	0	1/2	0	0.0042(2)
O1	0.1267(6)	0.3132(9)	−0.0379(7)	0.023(1)
O2	0.1329(7)	0.0241(11)	1/4	0.008(2)
O3	0	0.4166(15)	1/4	0.011(2)

Table 3. Selected Interatomic Distances (Å), Bond Angles (deg), and Tolerance Factors for the *Cmcm* Structures of Ln_3OsO_7 (Ln = Sm, Eu, Gd)

	Sm_3OsO_7	Eu_3OsO_7	Gd_3OsO_7
Ln(1)−O(1)	2.710(6) (×4)	2.704(7) (×4)	2.700(8) (×4)
Ln(1)−O(2)	2.350(4) (×4)	2.355(4) (×4)	2.342(5) (×4)
Ln(2)−O(1)	2.392(4) (×2)	2.382(8) (×2)	2.365(6) (×2)
Ln(2)−O(1)	2.392(3) (×2)	2.404(5) (×2)	2.391(6) (×2)
Ln(2)−O(2)	2.258(6)	2.251(8)	2.253(8)
	2.267(6)	2.259(8)	2.255(7)
Ln(2)−O(3)	2.589(3)	2.582(4)	2.575(4)
Os−O(1)	1.956(5) (×4)	1.954(6) (×4)	1.955(6) (×4)
Os−O(3)	1.955(3) (×2)	1.961(4) (×2)	1.956(4) (×2)
O(1)−Os−O(3)	85.6(2)	85.4(3)	85.0(3)
	94.4(2)	94.6(3)	95.0(3)
O(3)−Os−(O3)	180.0	180.0	180.0
Os−O(3)−Os	144.8(5)	143.7(6)	143.2(6)

samples at a rate of 2 °C/min under flowing air up to a temperature of 300 °C.

Magnetic Susceptibility. The magnetic susceptibility of the Ln_3OsO_7 (Ln = Sm, Eu, Gd) compounds was measured using a Quantum Design MPMS XL SQUID magnetometer. For the magnetic measurements, loose crystals of each osmate were placed into a gelatin capsule, which was placed inside a plastic straw. Samples were measured under both zero-field-cooled (ZFC) and field-cooled (FC) conditions. For all compounds, the magnetization was measured in the temperature range of 2−300 K. Susceptibility data were obtained in applied fields ranging from 100 G to 40 kG. In addition, field sweeps were recorded at various temperatures for the Eu_3OsO_7 and Gd_3OsO_7 compounds. The very small diamagnetic contribution of the gelatin capsule containing the sample had a negligible contribution to the overall magnetization, which was dominated by the sample signal.

Results and Discussion

Orthorhombic *Cmcm* Structures. Small black crystals, averaging 0.1−0.2 mm in length, were isolated from a molten hydroxide flux and used for single-crystal X-ray diffraction measurements. An analysis of the single-crystal diffraction data at room temperature for Sm_3OsO_7 and 380 and 480 K for Eu_3OsO_7 and Gd_3OsO_7, respectively, confirmed that all three compounds crystallize in the space group *Cmcm* commonly reported for the Ln_3MO_7 family of oxides. This high-temperature orthorhombic *Cmcm* structure, Figure 1, features chains of trans vertex-sharing OsO_6 octahedra that run along the *c*-axis. One-third of the lanthanide cations, Ln(1), are in a distorted cubic 8-fold coordination environment, forming chains of edge-sharing $Ln(1)O_8$ pseudocubes that concomitantly share edges with the chains of the OsO_6 octahedra, generating slabs that lie parallel to the *bc* plane. The remaining lanthanide cations, Ln(2), are located between these layers, where they exist in a 7-fold distorted pentagonal bipyramidal coordination environment.

The Os−O bond distances are in the ranges of 1.956(6)−1.957(3), 1.954(6)−1.961(4), and 1.955(6)−1.956(4) Å for Sm_3OsO_7, Eu_3OsO_7, and Gd_3OsO_7, respectively. These values agree well with previously reported values for Os^{5+} in octahedral coordination.[3,34,35] All crystallographic data and atomic positions for the high-temperature *Cmcm* structures are listed in Tables 1 and 2, respectively. Selected interatomic distances and angles are listed in Table 3.

Orthorhombic *P*2$_1$*nb* Structures. Recently, we reported on the synthesis and single-crystal X-ray diffraction structure determination of the high- and low-temperature structures of Ln_3RuO_7 (Ln = Sm, Eu); these compounds undergo a structure transition from space group *Cmcm* to *P*2$_1$*nb* at 190

Table 4. Crystallographic Data and Structure Refinement for the *P*2$_1$*nb* Structure of Ln_3OsO_7 (Ln = Sm, Eu, Gd)

	Sm_3OsO_7	Eu_3OsO_7	Gd_3OsO_7
fw (g/mol)	753.25	758.08	773.95
space group	P2$_1$*nb*	P2$_1$*nb*	P2$_1$*nb*
temp (K)	100	150	150
unit cell dimensions			
a (Å)	10.7627(3)	10.7030(4)	10.6459(5)
b (Å)	14.7725(5)	14.7385(5)	14.7450(7)
c (Å)	7.4334(2)	7.4143(3)	7.3879(4)
V (Å^3)	1181.85(6)	1169.58(8)	1159.71(10)
Z	8	8	8
density$_{calcd}$ (mg m^{-3})	8.467	8.610	8.866
abs coeff (mm$^{-1)}$	50.786	53.371	55.688
reflns collected	21990	15660	18487
independent reflns	4252 (R_{int} = 0.0554)	4132 (R_{int} = 0.0531)	4967 (R_{int} = 0.0422)
GOF on F^2	1.175	1.071	1.081
final R indices [$I > 2\sigma(I)$]	R1 = 0.0391, wR2 = 0.0754	R1 = 0.0456, wR2 = 0.1010	R1 = 0.0391, wR2 = 0.0892
R indices (all data)	R1 = 0.0500, wR2 = 0.0808	R1 = 0.0583, wR2 = 0.1089	R1 = 0.0441, wR2 = 0.0928
extinction coeff	0.00185(13)	0.00133(5)	0.00259(7)
residual electron density (e$^-$ Å^{-3})	3.195 and −3.624	2.454 and −3.338	4.194 and −4.478

Table 5. Atomic Coordinates and Equivalent Isotropic Parameters for the $P2_1nb$ Structure of Ln_3OsO_7 (Ln = Sm, Eu, Gd)

	x	*y*	*z*	U_{eq} (Å^2)
		Sm_3OsO_7		
Sm(1)	0.1871(2)	0.1362(1)	0.5024(1)	0.006(1)
Sm(2)	0.1736(2)	0.1133(1)	0.0018(1)	0.007(1)
Sm(3)	0.3999(1)	0.4762(1)	0.7626(1)	0.004(1)
Sm(4)	0.4585(1)	0.2275(1)	0.7433(1)	0.008(1)
Sm(5)	0.4482(2)	0.5275(1)	0.2521(1)	0.001(1)
Sm(6)	0.4115(1)	0.2728(1)	0.2454(1)	0.002(1)
Os(1)	0.1805(1)	0.3748(1)	0.4986(1)	0.006(1)
Os(2)	0.1785(1)	0.3736(1)	0.9978(1)	0.005(1)
O(1)	0.1880(17)	0.3357(9)	0.2494(8)	0.003(2)
O(2)	0.1710(20)	0.4163(12)	0.7488(10)	0.014(3)
O(3)	0.3098(10)	0.2828(9)	0.5360(14)	0.009(2)
O(4)	0.0557(9)	0.2797(8)	0.5344(13)	0.006(2)
O(5)	0.0528(10)	0.4694(9)	0.4606(13)	0.008(2)
O(6)	0.3082(10)	0.4674(9)	0.4668(13)	0.010(2)
O(7)	0.3284(9)	0.3072(7)	−0.0466(12)	0.009(2)
O(8)	0.0723(10)	0.2658(8)	−0.0365(14)	0.011(2)
O(9)	0.0240(10)	0.4398(8)	0.0426(13)	0.011(2)
O(10)	0.2817(9)	0.4841(7)	0.0391(12)	0.006(2)
O(11)	0.5491(15)	0.3681(10)	0.7579(11)	0.006(3)
O(12)	0.3093(15)	0.1193(10)	0.7639(12)	0.007(3)
O(13)	0.3091(15)	0.1423(12)	0.2358(13)	0.014(3)
O(14)	0.5455(15)	0.3954(9)	0.2353(11)	0.003(2)
		Eu_3OsO_7		
Eu(1)	0.1875(3)	0.1357(1)	0.5015(1)	0.007(1)
Eu(2)	0.1739(3)	0.1143(1)	0.0029(1)	0.007(1)
Eu(3)	0.4007(3)	0.4767(1)	0.7619(1)	0.004(1)
Eu(4)	0.4575(2)	0.2281(1)	0.7436(1)	0.008(1)
Eu(5)	0.4479(2)	0.5262(1)	0.2514(1)	0.009(1)
Eu(6)	0.4117(1)	0.2778(1)	0.2457(1)	0.003(1)
Os(1)	0.1803(2)	0.3748(1)	0.4977(1)	0.004(3)
Os(2)	0.1783(2)	0.3737(1)	0.9985(10)	0.004(1)
O(1)	0.1890(2)	0.3361(10)	0.2483(12)	0.011(3)
O(2)	0.1733(17)	0.4176(10)	0.7502(10)	0.006(3)
O(3)	0.3107(11)	0.2820(9)	0.5370(16)	0.007(2)
O(4)	0.0588(11)	0.2798(9)	0.5353(16)	0.006(2)
O(5)	0.0537(12)	0.4695(9)	0.4594(16)	0.009(2)
O(6)	0.3125(11)	0.4675(9)	0.4674(16)	0.007(2)
O(7)	0.3290(12)	0.3073(8)	−0.0457(16)	0.011(2)
O(8)	0.0737(11)	0.2666(7)	−0.0373(15)	0.005(2
O(9)	0.0256(13)	0.4405(9)	0.0446(18)	0.018(3)
O(10)	0.2848(13)	0.4827(9)	0.0397(17)	0.013(3)
O(11)	0.5514(19)	0.3654(11)	0.7571(14)	0.010(4)
O(12)	0.3095(16)	0.1196(9)	0.7638(14)	0.003(3)
O(13)	0.3117(17)	0.1438(13)	0.2359(16)	0.012(3)
O(14)	0.5464(14)	0.3933(11)	0.2352(13)	0.003(2)
		Gd_3OsO_7		
Gd(1)	0.1884(2)	0. 1371(1)	0. 5019(1)	0.006(1)
Gd(2)	0.1727(2)	0. 1125(1)	0.0029(1)	0.006(1)
Gd(3)	0.4003(1)	0. 4792(1)	0. 7629(1)	0.003(1)
Gd(4)	0.4589(1)	0. 2283(1)	0. 7429(1)	0.007(1)
Gd(5)	0.4473(1)	0. 5274(1)	0. 2513(1)	0.007(1)
Gd(6)	0.4125(1)	0. 2763(1)	0. 2445(1)	0.002(1)
Os(1)	0.1802(1)	0. 3749(1)	0. 4977(1)	0.003(1)
Os(2)	0.1782(1)	0. 3736(1)	0. 9983(1)	0.003(1)
O(1)	0. 1940(13)	0. 3335(6)	0. 2481(7)	0.007(2)
O(2)	0. 1742(11)	0. 4159(6)	0. 7482(7)	0.005(2)
O(3)	0. 3112(7)	0. 2814(5)	0. 5362(10)	0.004(1)
O(4)	0.0572(8)	0. 2788(7)	0. 5321(11)	0.010(2)
O(5)	0. 533(8)	0. 4680(6)	0. 4588(10)	0.008(1)
O(6)	0. 3084(8)	0. 4688(6)	0. 4680(10)	0.008(1)
O(7)	0. 3324(7)	0. 3097(5)	−0.0473(10)	0.008(1)
O(8)	0.0763(7)	0. 2640(5)	−0.0382(10)	0.005(1)
O(9)	0.0217(8)	0. 4374(6)	0.0422(10)	0.012(1)
O(10)	0. 2814(8)	0. 4839(6)	0.0386(10)	0.008(1)
O(11)	0. 5498(11)	0. 3683(7)	0. 7587(9)	0.005(2)
O(12)	0. 3112(12)	0. 1212(7)	0. 7587(9)	0.009(2)
O(13)	0. 3122(11)	0. 1433(8)	0. 2322(10)	0.009(2)
O(14)	0. 5445(9)	0. 3946(6)	0. 2358(9)	0.002(1)

Table 6. Average Interatomic Distances and Selected Bond Angles for the $P2_1nb$ Structure of Ln_3OsO_7 (Ln = Sm, Eu, Gd)

	Sm_3OsO_7	Eu_3OsO_7	Gd_3OsO_7
Ln(1)−O	2.434	2.426	2.420
Ln(2)−O	2.428	2.425	2.409
Ln(3)−O	2.407	2.395	2.385
Ln(4)−O	2.400	2.391	2.385
Ln(5)−O	2.381	2.375	2.370
Ln(6)−O	2.390	2.376	2.360
Os(1)−O	1.961	1.961	1.957
Os(2)−O	1.957	1.950	1.952
Os(1)−O(2)−Os(2)	142.6(10)	141.8(8)	143.1(5)
Os(2)−O(1)−Os(1)	145.6(7)	145.6(9)	142.8(5)

and 280 K, respectively.[5] In this paper, we report the high- and low-temperature single-crystal X-ray diffraction structures for the analogous osmates Ln_3OsO_7 (Ln = Sm, Eu, Gd). Sm_3OsO_7 was previously reported as a polycrystalline powder, with no information concerning a low-temperature structure.[12] At temperatures above 235, 330, and 430 K the Sm_3OsO_7, Eu_3OsO_7, and Gd_3OsO_7 compounds, respectively, exist in the expected orthorhombic fluorite-related structure, space group *Cmcm*. At temperatures below 235 K for Sm_3OsO_7 and at room temperature for Eu_3OsO_7 and Gd_3OsO_7,

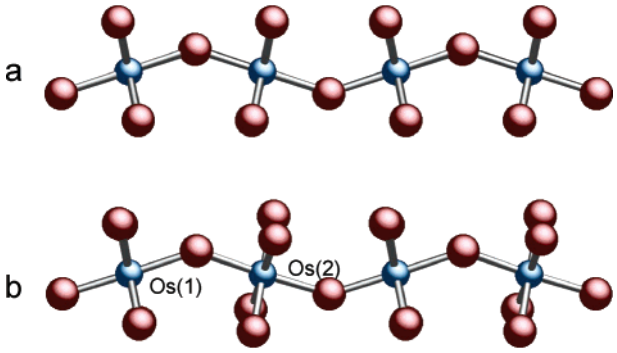

Figure 3. Views of the OsO_6 octahedral chains down the *a* axis for (a) the high-temperature structure and (b) the low-temperature structure of Ln_3OsO_7 (Ln = Sm, Eu, Gd). Note the distortion of the chains in the low-temperature structure as the octahedra now tilt in both the *bc* and *ab* planes.

numerous reflections in the diffraction pattern are present, indicative of the $P2_1nb$ structure.[5] The structure transition from *Cmcm* to $P2_1nb$ involves a distortion in the trans vertex-sharing OsO_6 chains that causes a doubling of the orthorhombic *b* axis and a concomitant reduction in the coordination environment of the Ln(1, 2) cations from 8 to 7. All crystallographic data and atomic positions for the low-temperature structures are listed in Tables 4 and 5, respec-

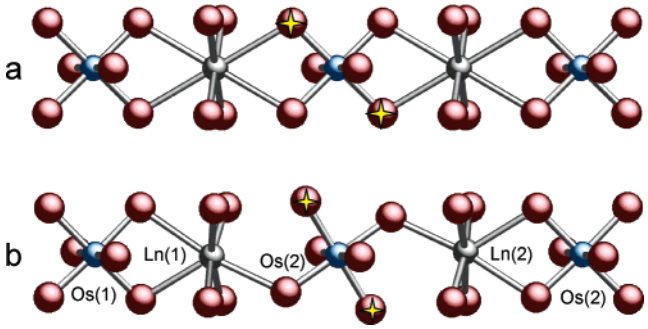

Figure 4. Coordination environments for the chains of OsO_6 octahedra and $Ln(1)O_8$ pseudo-cubes in the (a) high-temperature structure and Os(1, 2)O_6 octahedra and Ln(1, 2)O_7-capped trigonal prisms in the (b) low-temperature structure. The corresponding oxygen atoms found in different positions in each of the two structures are marked in red. In the low-temperature structure, the tilting of the Os(2)O_6 octahedra causes the reduction in coordination in the Ln(1, 2)O_7-capped trigonal prisms while the Os(1)O_6 octahedra maintain their edge-sharing connectivity to the Ln-(1, 2)O_7-capped trigonal prisms.

tively. Selected interatomic distances and angles are listed in Table 6.

The low-temperature structures are best described in the acentric primitive orthorhombic space group $P2_1nb$ with 6 independent rare earth positions, 2 unique osmium sites, and 14 independent oxygen atomic positions. Figure 3 shows the structure of the low-temperature forms of Ln_3OsO_7 (Ln = Sm, Eu, Gd). Similar to the high-temperature *Cmcm* phase, the structure features chains of vertex-shared OsO_6 octahedra running along the *c* axis which now, however, are tilted in the *ab* plane along the chain direction as well as in the *bc* plane. This additional tilting of the chain and associated rotation of the OsO_6 octahedra (Figure 3) has the effect of reducing the coordination environment of the associated Ln^{3+} polyhedra [now Ln(1) and Ln(2) in $P2_1nb$] from 8 to 7 (Figure 4). In the high-temperature *Cmcm* structure, the chains of trans vertex-sharing OsO_6 octahedra connect to the chains of edge-sharing $Ln(1)O_8$ pseudocubes via pairs of equatorial OsO_6 oxygens. In the low-temperature $P2_1nb$ structure, however, the tilting of the OsO_6 chains in the *ab* plane and the concomitant rotation of the Ru(2)O_6 octahedra cause one of the equatorial oxygens [Ln(1)−O(9) and Ln-(2)−O(7) in $P2_1nb$] to rotate away from the lanthanide cation (from ∼2.70 to ∼3.38 Å), while the other three oxygens [Ln-(1)−O(3), O(4), O(10) and Ln(2)−O(5), O(6), O(8)] move closer. The other Ln(2)−O distances are not affected and remain within ∼0.05 Å of their values in the *Cmcm* structure. The Ln(1)−O(9) and Ln(2)−O(7) distances of about 3.38 Å are greater that the sum of the ionic radii and are thus considered nonbonding, reducing the coordination environment from 8 to 7 (Figure 4). The coordination environment of the lanthanide is now best described as a capped trigonal

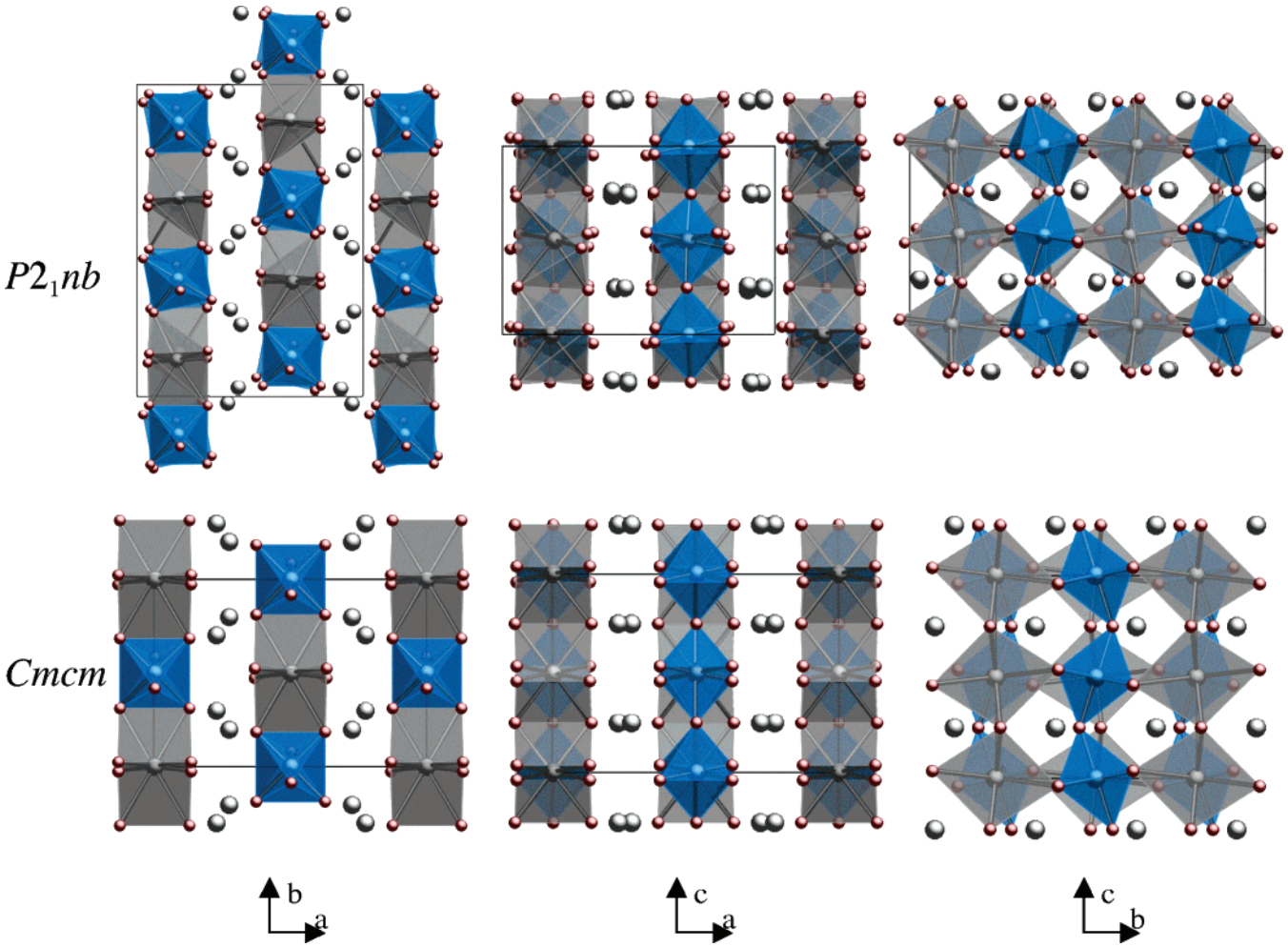

Figure 5. Comparative orientations of the high- and low-temperature structures viewed down each of the crystallographic axes.

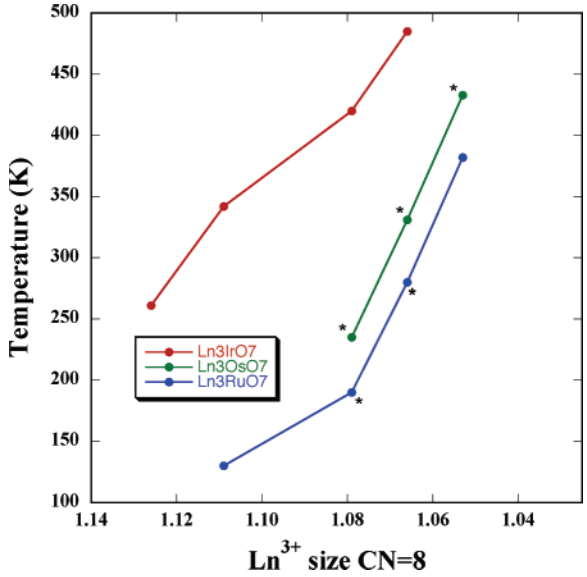

Figure 6. Structure transition temperatures for the compounds Ln_3MO_7 (Ln = Ln^{3+}, M = Ir, Os, Ru) as determined by thermal and magnetic characterization.[27−30] Above the marker, the compound exists in the high-temperature *Cmcm* structure, and below the marker the compound exists in a low-temperature structure. Compositions investigated by us are denoted with an asterisk. The phases Ln_3RuO_7 (Ln = Sm, Eu)[5] and Ln_3OsO_7 (Ln = Sm, Eu, Gd) exist in the $P2_1nb$ low-temperature structure reported in this paper, as determined from single-crystal X-ray diffraction.

prism. It should be noted that the $Os(1)O_6$ octahedra maintain their edge-sharing connectivity with both Ln(1) and Ln(2), and it is only the rotation of the $Os(2)O_6$ octahedra that causes the oxygen to move out of the Ln(1, 2) coordination sphere. The Os−O distances, on the other hand, are not affected by the structural distortion, and the average Os(1)−O and Os(2)−O distances are 1.961 and 1.957, 1.961 and 1.950, and 1.955 and 1.952 Å for Sm_3OsO_7, Eu_3OsO_7, and Gd_3OsO_7, respectively (Table 6). In the low-temperature structure, the OsO_6 chains still connect to the rare earth chains to form sheets (Figure 5), between which the remaining rare earth cations exist in four crystallographically unique sites, Ln(3)−Ln(6), as distorted pentagonal bipyramids. The Os−Ln−O slabs are more distorted in the low-temperature structure, which can be clearly seen in Figure 5, which shows the view down the *c* axis.

As mentioned above, the temperatures at which the title compounds undergo the structural phase transition are approximately 235, 330, and 430 K for Sm_3OsO_7, Eu_3OsO_7, and Gd_3OsO_7, respectively. Figure 6 shows the structure transition temperatures for the three series of related phases Ln_3MO_7 (M = Ru, Os, Ir), above which these compounds exist in the high-temperature *Cmcm* structure and below which they exist, at least for Ln_3RuO_7 (Ln = Sm, Eu)[5] and Ln_3OsO_7 (Ln = Sm, Eu, Gd) (this article), in the low-temperature $P2_1nb$ structure.

The structure transition appears to be influenced, at least in part, by the size of the Ln^{3+} cation. The transition temperature increases for each of the three series of compounds as the size of the Ln^{3+} cation decreases, and although each series is offset from one another, the general trend is similar and each transition temperature within a series is separated by approximately the same temperature interval

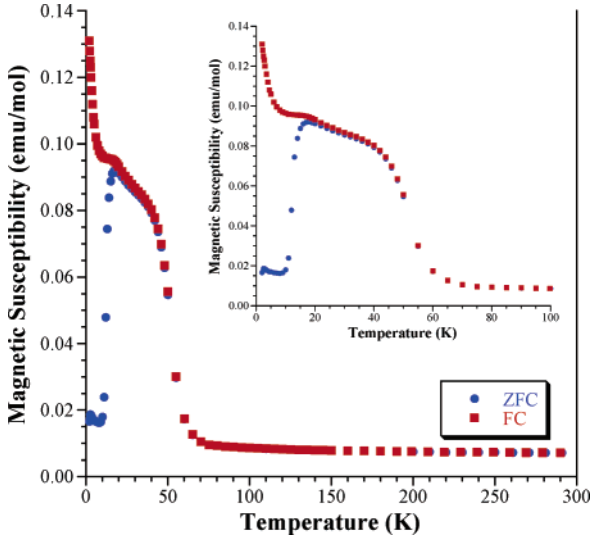

Figure 7. Temperature dependence of the susceptibility of Sm_3OsO_7 measured in an applied field of 10 kG.

of 100 K. The cause for the difference between the three series is more difficult to assign, as Ru^{5+}, Ir^{5+}, and Os^{5+} are very close in size, suggesting that it is not primarily a size effect.

TGA-DTA. The temperatures at which the Eu_3OsO_7 and Gd_3OsO_7 compounds undergo the structural phase transition from the low-temperature $P2_1nb$ structure to the high-temperature *Cmcm* structure were determined from the DTA traces from room temperature to 300 °C. Thermal events are detected at approximately 60 °C and 160 °C for Eu_3OsO_7 and Gd_3OsO_7, respectively, in the DTA data and are attributed to the structural phase transition. The TGA data showed no significant weight loss (<1%) up to 300 °C, and the DTA trace is included as supplemental information.

Magnetism. Sm_3OsO_7. The temperature dependence of the magnetic susceptibility for loose crystals of Sm_3OsO_7 in an applied field of 10 kG is shown in Figure 7. A series of complex magnetic transitions at ∼60, ∼50 and ∼20 K are apparent in the data and, while more pronounced, closely match those reported and discussed previously by Plaisier for data collected on polycrystalline powders of Sm_3OsO_7.[12] The curie constant for Sm_3OsO_7 cannot be calculated because up to the highest temperature measured (300 K) the magnetic behavior deviates from Curie−Weiss-type behavior.

Eu_3OsO_7. The temperature dependence of the magnetic susceptibility for Eu_3OsO_7 in an applied field of 10 kG is shown in Figure 8. As in Sm_3OsO_7, three magnetic transitions are observed at ∼60, ∼50 and ∼20 K, and the ZFC data undergo an antiferromagnetic-like downturn at about 40 K. Below 40 K, the data exhibits a field dependence, as evidenced by the fact that the ZFC and FC data no longer overlay. The high-temperature susceptibility data deviate significantly from Curie−Weiss-type behavior making it impossible to extract a magnetic moment. Figure 9 shows the field dependence of the magnetization at 150, 50, 10, and 2 K. It can be clearly seen that at temperatures below 50 K there exists a field dependence, albeit small. More interesting is the relatively small field dependence observed

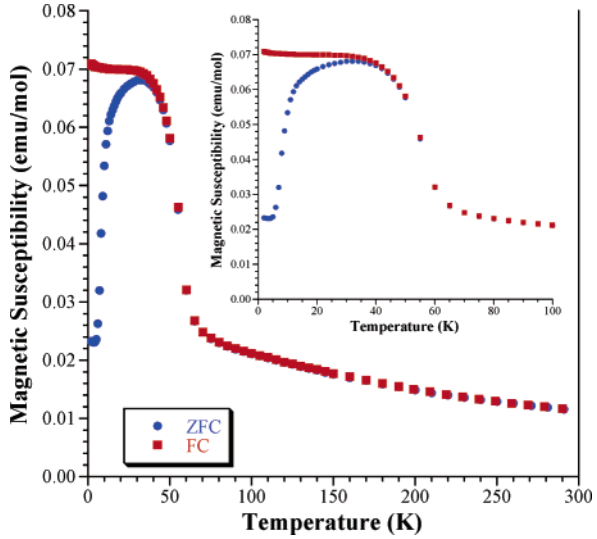

Figure 8. Temperature dependence of the susceptibility of Eu_3OsO_7 measured in an applied field of 10 kG.

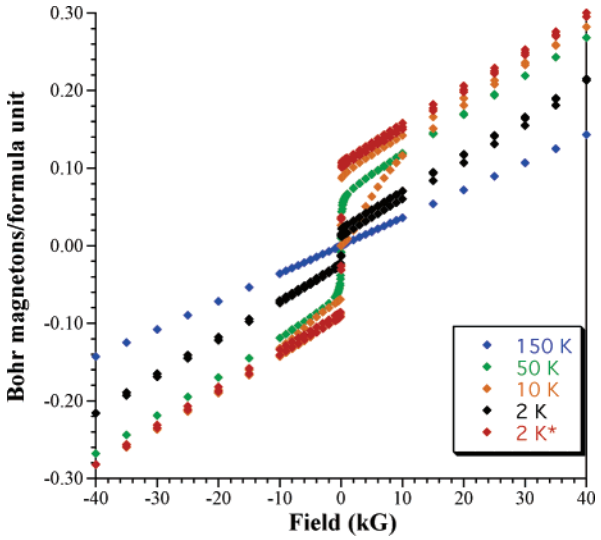

Figure 9. Field dependence of the magnetization of Eu_3OsO_7 measured at temperatures of 150, 50, 10, and 2 K (2 K* represents the field dependence measured at 2 K after heating to 50 K followed by cooling to 2 K all in an applied field of 40 kG).

at 2 K for a zero-field-cooled measurement (black diamonds). However, after the sample was heated to 50 °C and cooled back down to 2 K in an applied field of 40 kG, the field dependence becomes the largest relative to the other temperatures (red diamonds). This behavior is indicative of domain wall pinning and suggests that in the absence of sufficient thermal energy to allow the domain wall motion to align the spins in an external field, the overall magnetization of the sample cannot reach its maximum. To further illustrate this point, the magnetic susceptibility in a field of 100 G is presented in Figure 10. The data were collected in temperature loops from 2 K to X to 2 K (X = 30, 44, 50, 70 K). As the temperature increases, the domains grow and align in the external field, gradually increasing the overall susceptibility to a maximum. Warming the sample any further above the transition temperature at ~50 K will not increase the maximum susceptibility of ~3.5 emu/mole.

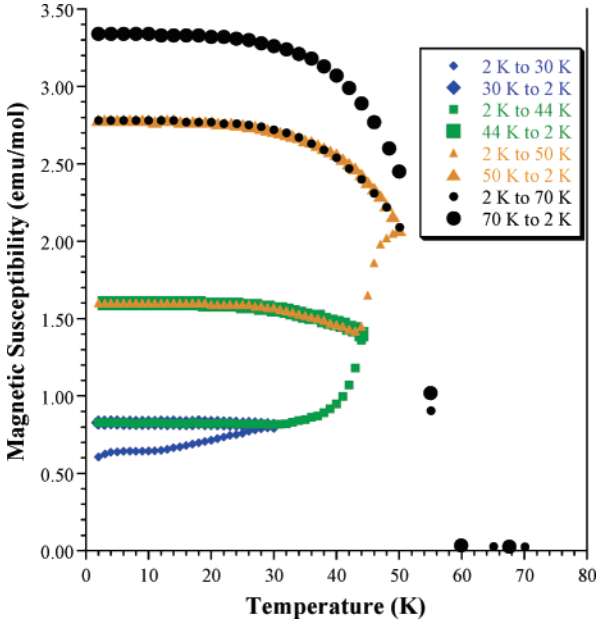

Figure 10. Temperature dependence of the susceptibility of Eu_3OsO_7 measured sequentially in an applied field of 100 G.

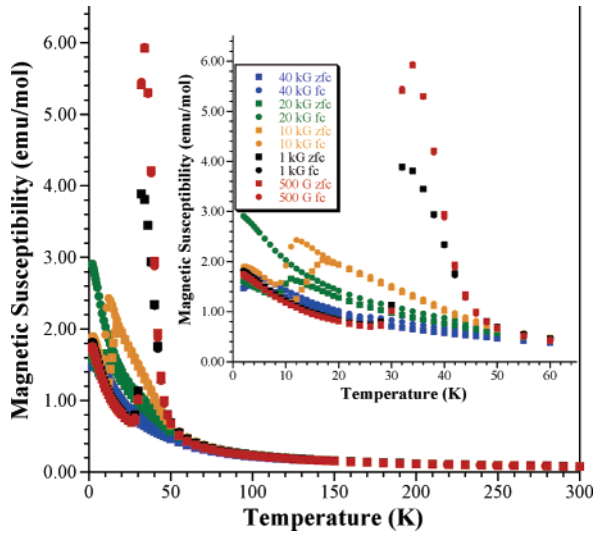

Figure 11. Temperature dependence of the susceptibility of Gd_3OsO_7 measured in applied fields of 0.5, 1, 10, 20, and 40 kG.

Gd_3OsO_7: The temperature dependence of the susceptibility for Gd_3OsO_7 in applied fields of 40, 20, 10, 1, and 0.5 kG is shown in Figure 11. Fitting the high-temperature susceptibility (100 < T > 300 K) measured in an applied field of 10 kG to the Curie−Weiss law results in values of μ_{eff} = 13.7, C = 23.6 emu K mole^{-1}, μ_B, θ = 1.6 K which is slightly lower than the expected value of μ = 14.2 μ_B. (The expected value can be estimated as 14.2 using the reported moment for octahedral Os(V) of μ_{eff} = 3.26 μ_B in La_2NaOsO_6[3] and a value of μ_{eff} = 8.0 μ_B for Gd^{3+}.) The slightly positive Weiss constant is indicative of weak ferromagnetic interactions, and the plot of the susceptibility as a function of temperature does indeed show an ordered ferromagnetic-like state at low fields (below 10 kG) at 34 K (Figure 10). Similar magnetized states have been observed in the pillared perovskite $La_5Re_3MnO_{16}$ and have been

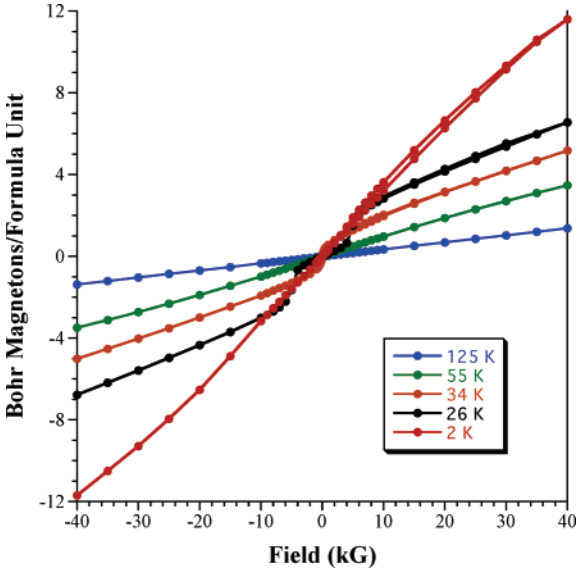

Figure 12. Field dependence of the magnetization of Gd_3OsO_7 measured at temperatures of 125, 55, 34, 26, and 2 K.

attributed to an ordered, magnetized state.[36] The field dependence of the magnetization recorded at 125, 55, 34, 26, and 2 K is shown in Figure 12. Well above the ordering temperature of 34 K, paramagnetic-like behavior is observed. At 34 K, a slight field dependence is observed, and at lower temperatures the field dependence increases to a moment of about 12 μ_B at 2 K and 40 kG, however the behavior does not indicate saturation.

Summary

The three fluorite-related osmates of the Ln_3OsO_7 (Ln = Sm, Eu, Gd) stoichiometry were synthesized in single-crystal form, their structures were characterized, and their magnetic properties were investigated. The growth of these oxides from molten hydroxide fluxes further establishes these melts as a successful solvent system for the preparation of oxide structures containing both lanthanides and platinum group metals. The structural transitions at approximately 235, 330, and 430 K for Sm_3OsO_7, Eu_3OsO_7, and Gd_3OsO_7, respectively, result in a loss of lattice centering, a doubling of the *b* axis, and a reduction in the coordination of one of the Ln sites from 8-fold to 7-fold. The low-temperature structure of Sm_3OsO_7 and the high- and low-temperature structures of Eu_3OsO_7 and Gd_3OsO_7 have been completely characterized by single-crystal X-ray diffraction. Sm_3OsO_7 and Eu_3OsO_7 exhibit complex magnetic behavior below about 50 K. Gd_3OsO_7 shows ferromagnetic-like order at 34 K in applied fields of less than 10 kG and also exhibits Curie−Weiss-type behavior at high temperatures ($T > 100$ K) with an effective moment of 13.7 μ_B.

Acknowledgment. This work was supported by the Department of Energy through Grant DE-FG02-04ER46122 and the National Science Foundation through Grants DMR: 0134156 and DMR:0450103.

Supporting Information Available: Additional structural and crystallographic data and differential thermal analysis (DTA) data. This material is available free of charge via the Internet at http://pubs.acs.org.

IC0506106